



CoP/Co₂P heterostructure in N, P co-doped carbon nanofibers enable superior lithium storage via the built-in electric field

Xuxu Wang¹, Cairan Yue¹, Wenbo Wang¹, Fen Yao^{1,*}, Jinhui Li¹, Weijie Zhu^{2,*}, Ping Nie¹, Limin Chang^{1,*}

Keywords:

Cobalt phosphide, heterostructure, built-in electric field, N, P co-doped carbon, lithium-ion batteries

Citation:

Wang, X.; Yue, C.; Wang, W.; Yao, F.; Li, J.; Zhu, W.; Nie, P.; Chang, L. CoP/Co₂P heterostructure in N, P co-doped carbon nanofibers enable superior lithium storage via the built-in electric field. *Energy Mater.* 2026, 6, 600032. <https://dx.doi.org/10.20517/energymater.2025.191>

Received: 7 Nov 2025

First Decision: 17 Dec 2025

Revised: 11 Jan 2026

Accepted: 20 Jan 2026

Published: 7 Apr 2026

Academic Editor:

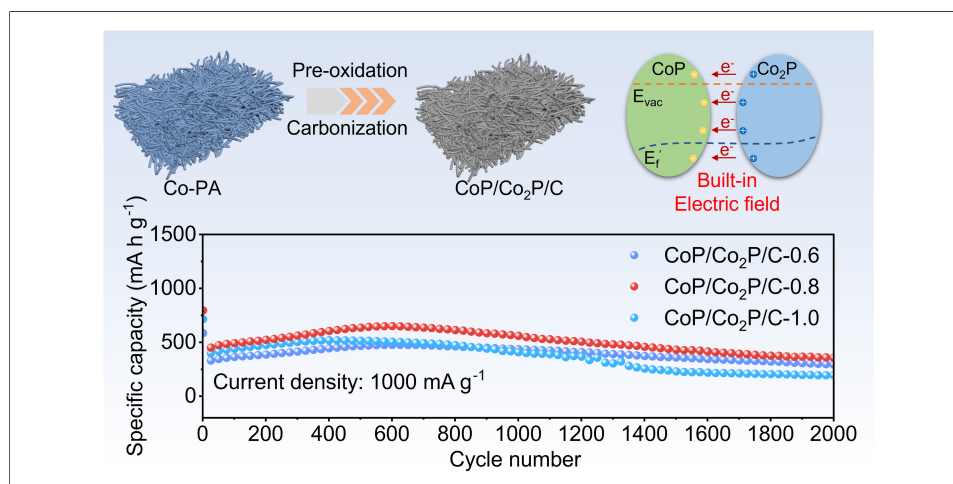
Federico Bella

Copy Editor:

Shu-Yuan Duan

Production Editor:

Shu-Yuan Duan



Abstract

Transition metal phosphides (TMPs) have garnered significant attention as anode for lithium-ion batteries (LIBs) owing to their high theoretical capacity and moderate Li-intercalation potential. However, TMP still suffer from challenges, including severe volume effects and poor electrical conductivity. Herein, the heterostructure nanofibers anode is synthesized by uniformly distributing CoP/Co₂P nanoparticles onto N, P co-doped carbon substrate (CoP/Co₂P/C). The built-in electric field generated by the heterostructure enhances electron/ion conductivity, provides additional Li storage sites, thereby optimizing electrochemical performance. The CoP/Co₂P/C nanofibers exhibit great cycling stability in applications as LIBs anodes, maintaining the specific capacity above 356 mA h g⁻¹ after 2000 cycles under 1,000 mA g⁻¹. By regulating the ratio of CoP to Co₂P, the numbers of heterostructure within the nanofibers were effectively controlled. Based on this, the correlation between heterostructure and electrochemical performance was analyzed. The strategy of constructing heterostructure using the same metal

¹Key Laboratory of Preparation and Applications of Environmentally Friendly Material of the Ministry of Education & College of Chemistry, Jilin Normal University, Changchun 130103, Jilin, China.

²Electrocatalysis and New Energy Materials Research Center, School of Materials Engineering, Suzhou University of Technology, Suzhou 215500, Jiangsu, China.

*Correspondence to: Fen Yao, Limin Chang, Key Laboratory of Preparation and Applications of Environmentally Friendly Material of the Ministry of Education & College of Chemistry, Jilin Normal University, Changchun 130103, Jilin, China. E-mail: yaof@jlnu.edu.cn; changlimin2139@163.com; Weijie Zhu, Electrocatalysis and New Energy Materials Research Center, School of Materials Engineering, Suzhou University of Technology, Suzhou 215500, Jiangsu, China. E-mail: zhuweijie@szut.edu.cn

significantly simplified the preparation process for high-performance TMPs anode, providing a viable approach for developing novel anode for LIBs.

INTRODUCTION

Solar energy, as the most abundant renewable resource, holds the key to breaking free from fossil fuels, mitigating climate change, and safeguarding energy security. However, its inherent intermittency limits widespread application. Efficient energy storage is crucial for establishing a continuous, stable and dispatchable energy supply network. Owing to the high energy/power density and long cycle lifespan, lithium-ion batteries (LIBs) account for a dominant share of the current energy storage market^[1,2]. However, constrained by the lower theoretical specific capacity of graphite anodes (372 mA h g^{-1}), the electrochemical performance of lithium-ion batteries requires further improvement. Therefore, it is imperative to develop anode for LIBs that exhibit high specific capacity and stable cycling performance^[3-5].

Transition metal phosphides (TMPs) are considered promising anode, primarily due to their high theoretical specific capacity and suitable voltage plateau^[6-9]. The cycling stability and rate performance of TMPs requires improvement. This is due to the poor conductivity and significant volume effect of TMPs^[10-14]. Several approaches have been developed to improve the electrochemical performance of TMPs, such as designing nanostructure, compositing with carbon materials, and preparing porous structures. First, the introduction of nanostructures facilitates faster transport of Li^+ and electrons by shortening their diffusion distance, and avoid pulverization caused by volume effects and enhance the electrochemical performance of TMPs. Second, designing TMPs as composites with conductive materials can overcome their shortcomings in conductivity^[15,16]. In addition, carbon also can keep the anode structurally intact during severe volume changes, thereby extending the cycle life of the electrode. Another effective approach to improve the electrochemical performance of TMPs is design porous structures. The porous structure prevents pulverization of TMPs during charging and discharging, significantly enhancing cycle stability^[17]. Porous structure also increases the electrochemical reaction area, accelerating Li^+ diffusion at the electrode-electrolyte interface.

In addition to these strategies, introduction of heterostructure also serves as a feasible measure to optimize the electrochemical performance of TMPs. The introduction of heterostructure is able to modify the crystal and electronic structures, generating numerous defects and lattice distortions, and inducing the built-in electric field (BIEF). This provides additional active sites and Li^+ transport channels^[18]. Additionally, heterostructures can prevent powdering caused by volume effects, thereby enhancing the cycling stability of the anode. Finally, the heterostructure can combine the advantages of different materials to achieve optimal electrochemical performance. For instance, Xiao *et al.* synthesized the hierarchical hybrid anode $[\text{Co}(\text{OH})_2/\text{Ni}_2\text{P@N-C}]$ by uniformly dispersing N-doped carbon coated Ni_2P nanoparticles on $\text{Co}(\text{OH})_2$ nanosheets. This unique hybrid structure enhances electron/ion conductivity, resulting in superior electrochemical performance as an anode material compared to $\text{Ni}_2\text{P@N-C}$ ^[19]. Li *et al.* optimized the electrochemical performance of TMPs by the BIEF formed at the FeP/SnP heterointerface^[20]. The study found that this BIEF not only optimizes the electrochemical reaction kinetics but also provides additional active sites. When used as the anode for LIBs, the FeP/SnP heterostructure exhibits outstanding electrochemical performance. However, the heterostructure of multi-metal phosphides typically require complex synthesis processes. Constructing such heterostructure using phosphides of the same metal but with different stoichiometric ratios holds promise for significantly simplifying the preparation process while retaining the excellent electrochemical performance. As the typical example of TMPs, cobalt phosphide exhibits multiple thermodynamically stable compounds such as Co_2P , CoP , CoP_2 and CoP_3 ^[7,21-23]. Among these, Co_2P belongs to the hexagonal crystal system. It is rich in metallic cobalt-cobalt bonds, thereby

exhibiting excellent electronic conductivity; however, its theoretical specific capacity is relatively low. Although CoP, which belongs to the orthorhombic crystal system, possesses the higher theoretical specific capacity, its electrochemical performance is limited by its poor intrinsic conductivity and the severe volume effect during charge/discharge process^[21]. Therefore, constructing CoP/Co₂P heterostructure is expected to simplify the preparation process and achieve outstanding electrochemical performance.

Herein, CoP/Co₂P nanoparticles onto N, P co-doped carbon substrate (CoP/Co₂P/C) nanofibers are synthesized via the facile electrospinning and thermal reduction process. By controlling the amounts of Co²⁺ and phytic acid (PA), the ratio of Co₂P to CoP can be altered, thereby obtaining nanofibers with varying heterostructure contents. The difference in work function between CoP and Co₂P induces electron transfer at the heterointerface, resulting in the BIEF, which provides the electron/ion transport channels and creates novel active sites^[18]. Moreover, the abundant N, P co-doped carbon (NPC) significantly improves the conductivity of the TMPs, alleviates mechanical stress caused by volume changes, thereby enables TMPs anodes with long lifespan and excellent rate performance. When used as anode for LIBs, CoP/Co₂P/C nanofibers show great electrochemical performance. At the current density of 1,000 mA g⁻¹, the specific capacity of CoP/Co₂P/C remained above 356 mA h g⁻¹ after 2,000 cycles, demonstrating long cycle lifespan and excellent high-current charge/discharge capability. This result shows that the heterostructure composed of TMPs with different stoichiometric ratios of the same metal can combine the advantages of both TMPs, making it a promising anode material for high-performance LIBs. This simple heterostructure preparation method is also expected to be applicable to the design of other anodes.

EXPERIMENTAL

Synthesis of Co-PA nanofibers

First, the PA (0.424 g) was added into dimethylformamide (DMF, 10 mL) and stirred at 80 °C. Next, added polyacrylonitrile (PAN, 0.8 g) and stirred for 4 h. Then, a quantity of CoCl₂·6H₂O was added and stirred for 12 h, resulting in the electrospinning solution. Finally, electrospinning was performed at 15kV^[22]. When the mass of CoCl₂·6H₂O in the electrospinning solution was 0.4, 0.6, 0.8 and 1.0 g were named Co-PA-n (n is the mass of CoCl₂·6H₂O).

Synthesis of CoP/Co₂P/C nanofibers

Firstly, the Co-PA film was pre-oxidized at 250 °C. Subsequently, carbonize it for 3 h in the Ar atmosphere under 800 °C. The resulting product was named as CoP/Co₂P/C-n (n is the mass of CoCl₂·6H₂O).

Synthesis of CoP/C nanofibers

To synthesize a single-phase CoP, Co-PA-0.4 was prepared using an electrospinning solution containing 0.4 g of CoCl₂·6H₂O. Following pre-oxidation and carbonization. The resulting product is CoP/C nanofibers.

RESULTS AND DISCUSSION

The synthesis process of nanofibers is illustrated in [Figure 1](#). First, the nanofibers film, containing the phosphorus source and CoCl₂, is prepared via electrospinning. Subsequently, the precursor undergoes pre-oxidation and carbonization. During this process, -PO₄ in PA reacts with Co²⁺ to form a CoP/Co₂P heterostructure. Additionally, the carbon-containing parts of PA and PAN are reduced to carbon substrate doped with N and P. This substrate tightly coats the surface of the CoP/Co₂P nanoparticles, ultimately forming CoP/Co₂P/C nanofibers.

Morphology and surface changes of the nanofibers during the preparation process is analyzed through scanning electron microscopy (SEM) characterization. As displayed in [Supplementary Figure 1](#), the

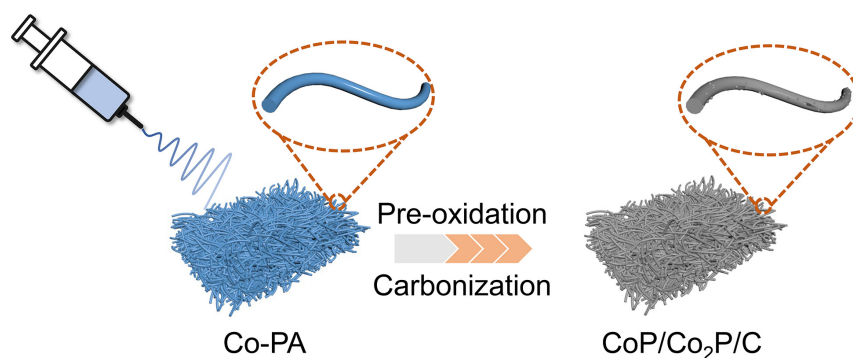


Figure 1. Schematic of the preparation process of CoP/Co₂P/C. PA: Phytic acid; CoP/Co₂P/C: CoP/Co₂P nanoparticles onto N, P co-doped carbon substrate.

morphology of the precursor is nanofibers, whose diameter is approximately 200 nm. The surface of nanofibers is smooth with no visible pores. To enhance the structural toughness of the nanofibers, they are subsequently subjected to the pre-oxidation treatment. The pre-oxidized samples exhibit the network structure composed of nanofibers [Supplementary Figure 2], which facilitates the formation of the conductive network. Finally, the nanofibers undergo high-temperature treatment to transform into the CoP/Co₂P/C. For CoP/Co₂P/C-0.8 [Figure 2A and B], it remains interconnected nanofibers. Additionally, there are nanoparticles uniformly distributed on the surface of nanofibers, the diameter of nanoparticles is approximately 20 nm. The small size of nanoparticles effectively relieves the significant volume change during the charge/discharge process, improving cycling stability. Additionally, numerous pores exist on the surface of nanofibers, which is beneficial for electrolyte infiltration and thus accelerates Li⁺ diffusion at the interface. The morphology of CoP/Co₂P/C-0.6 and CoP/Co₂P/C-1.0 is similar to CoP/Co₂P/C-0.8 [Supplementary Figure 3], also exhibiting nanofibers structures composed of CoP/Co₂P nanoparticles and carbon substrate.

The structure of CoP/Co₂P/C-0.8 is further characterized by transmission electron microscopy (TEM). As illustrated in the Figure 2C, CoP/Co₂P/C-0.8 nanofibers consist of uniformly sized nanoparticles and carbon, and carbon is tightly coated on the surface of the nanoparticles. In the high-resolution transmission electron microscopy (HRTEM) image [Figure 2D] of nanoparticles, distinct lattice fringes can be observed. The lattice fringe with the spacing of 1.902 Å corresponds to the (211) crystal plane of CoP, while the lattice fringe with the spacing of 2.079 Å corresponds to the (211) crystal plane of Co₂P. There is the significant interface between the two crystals, indicating the presence of the CoP/Co₂P heterostructure within the nanoparticles. Furthermore, the selected area electron diffraction (SAED) of the CoP/Co₂P/C-0.8 show diffraction spots belonging to CoP and Co₂P [Figure 2E], further confirming that the nanoparticles are composed of CoP and Co₂P. The energy dispersive X-ray spectroscopy (EDS) elemental mapping results of CoP/Co₂P/C-0.8 are given in Figure 2F. The surfaces of the samples contain C, N, P, and Co elements. Among these, C and N are uniformly dispersed throughout the nanofibers, while Co is concentrated on the nanoparticles. For P, distribution occurs not only on the nanoparticles but also on the carbon. This suggests that the nanofibers are consisted of the CoP/Co₂P heterostructure and NPC. Furthermore, the N element content is about 5.21 at% [Supplementary Figure 4]. The higher N doping concentration can introduce abundant defects into the carbon substrate, which contributes to enhancing the conductivity and lithium storage capacity of the nanofibers.

The composition of the nanofibers and the ratio of CoP to Co₂P are characterized through X-ray diffraction (XRD) analysis. As shown in the Figure 3A, diffraction peaks belonging to CoP and Co₂P are found in the

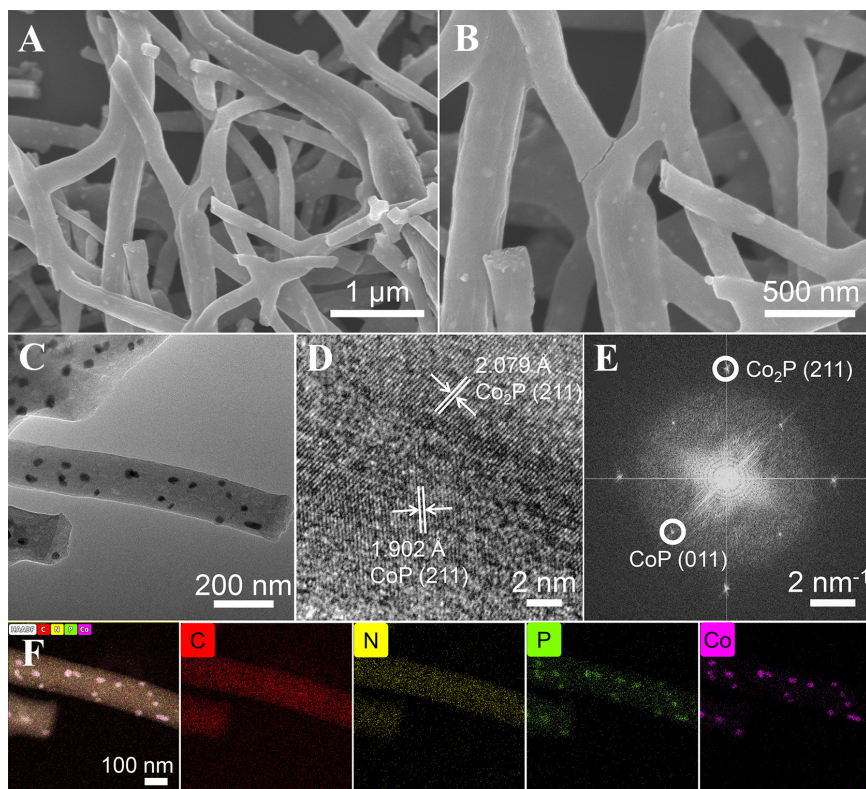


Figure 2. (A and B) SEM images; (C) TEM image; (D) HRTEM image; (E) SAED image; and (F) EDS elemental mapping of CoP/Co₂P/C-0.8. SEM: Scanning electron microscopy; TEM: transmission electron microscopy HRTEM: high-resolution transmission electron microscopy; SAED: selected area electron diffraction; EDS: energy dispersive X-ray spectroscopy.

XRD patterns of all three nanofibers. Interestingly, from the CoP/Co₂P/C-0.6 to CoP/Co₂P/C-1.0, the ratio of the intensity of the (211) crystal plane diffraction peak for Co₂P to that of the (211) crystal plane diffraction peak for CoP gradually increases. This indicates that as the ratio of Co²⁺ to PA increased, the Co₂P content in the nanofibers also gradually increased. Furthermore, the XRD patterns of the three nanofibers show no diffraction peaks from other substances, indicating that after the pre-oxidation and reduction processes, Co-PA has been completely converted into CoP/Co₂P/C nanofibers without producing any other impurities. In addition, the XRD pattern of CoP/C [Supplementary Figure 5] matches well with the standard CoP pattern, indicating high phase purity without impurity phases. Figure 3B shows the Raman spectra of three kinds of CoP/Co₂P/C nanofibers. The two peaks of Raman spectra are belonged to D peaks (belonging to disordered carbon) and G peaks (belonging to graphitic carbon), respectively. The ratio of D peaks to G peaks intensity (I_D/I_G) values of all CoP/Co₂P/C nanofibers fall within the range of 1.08–1.16. This indicates that the NPC of the nanofibers is all abundant in defects^[24,25]. These defects will provide a large number of Li⁺ adsorption sites, thereby enhancing the specific capacity of nanofibers. To analyze the thermal stability of the sample, nanofibers are tested by thermogravimetric analysis in the air [Supplementary Figure 6]. For CoP/Co₂P/C-0.8, the mass change is mainly attributed to the desorption of H₂O and air, the decomposition of carbon, and the oxidation of CoP/Co₂P^[21]. Calculations indicate that the content of nanoparticles in CoP/Co₂P/C-0.8 ranges between 28.8% and 31.8%. As the content of Co₂P in the nanofibers increases, the mass loss of nanofibers at 900 °C is primarily reduced. This is attributed to the increased content of Co₂P and decreased carbon content within the nanofibers.

X-ray photoelectron spectroscopy (XPS) measurements are performed on the nanofibers to analyze the valence states of chemical elements on their surfaces. As shown in Supplementary Figure 7, the CoP/Co₂P/C

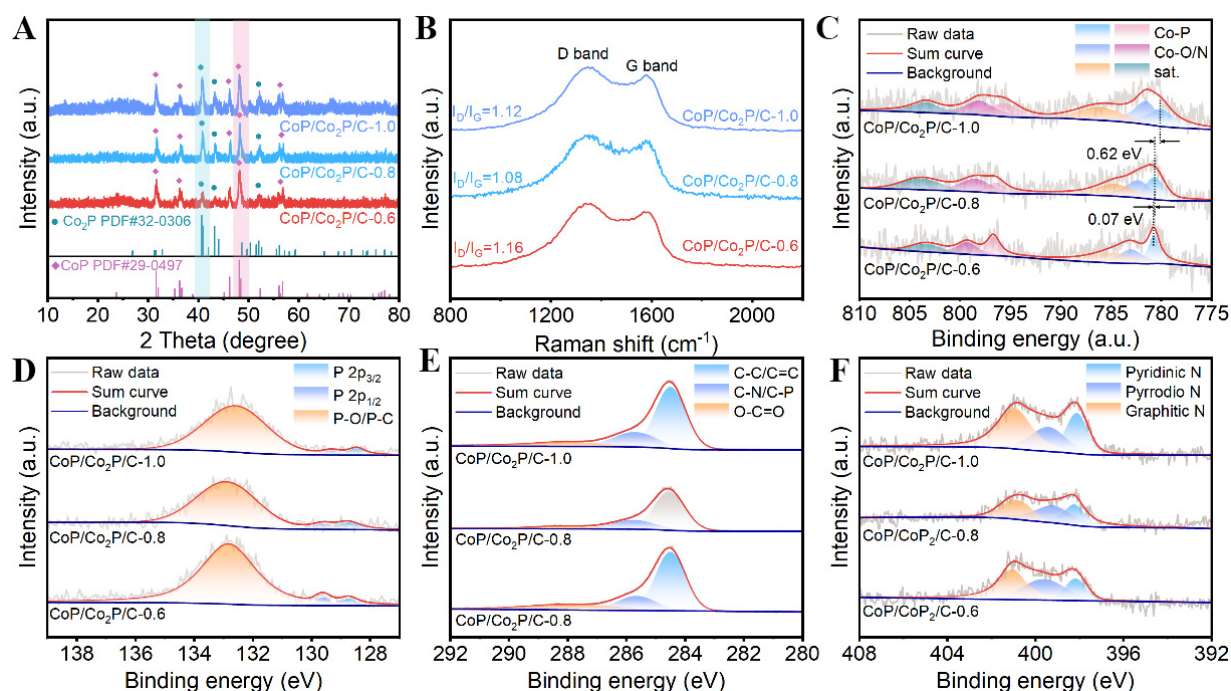


Figure 3. Structures and compositions of CoP/Co₂P/C nanofibers: XRD patterns (A); Raman spectra (B); high-resolution XPS survey spectra of Co 2p (C), P 2p (D), C 1s (E), and N 1s (F). CoP/Co₂P/C: CoP/Co₂P nanoparticles onto N, P co-doped carbon substrate; XRD: X-ray diffraction; XPS: X-ray photoelectron spectroscopy.

nanofibers contain Co, P, N and C elements. Figure 3C is the Co 2p high-resolution spectrum for CoP/Co₂P/C-0.8. The peaks at 780.69 eV and 796.40 eV represent the Co 2p_{3/2} and 2p_{1/2} orbitals of Co-P, respectively. The appearance of these peaks confirms the successful conversion of Co-PA into CoP/Co₂P. Additionally, peaks belonging to surface-oxidized cobalt (782 eV and 795 eV) are observed. This is common in metallic TMPs, mainly due to sample oxidation upon exposure to air^[26,27]. Importantly, as the increase of Co₂P content in CoP/Co₂P nanoparticles, the Co-P peak gradually shifts toward lower binding energy. This is attributed to electron transfer occurring at the CoP/Co₂P heterointerface, where the resulting BIEF will provide additional Li⁺ storage sites and fast diffusion channels for Li⁺. In the P 2p spectrum of CoP/Co₂P/C-0.8 [Figure 3D], P-Co peaks are observed with binding energies of 128.74 eV (P 2p_{3/2}) and 129.62 eV (P 2p_{1/2}). The presence of P-Co bonds suggests that after high-temperature reaction, Co²⁺ react with P from PA to form CoP/Co₂P. The peak at 132.88 eV correlates with the P-O/P-C bond. The P-O bond mainly results from the oxidation of CoP/Co₂P in air. The presence of P-C bonds indicates that phosphorus has been successfully doped into the carbon, which contribute to the electrical conductivity and lithium storage capacity of the nanofibers^[10]. The P 2p high-resolution spectra of CoP/Co₂P/C-0.6 and CoP/Co₂P/C-1.0 are similar to that of CoP/Co₂P/C-0.8. The slight shifts in peak positions are also attributed to electron transfer at the heterointerface. The high-resolution C 1s spectra of CoP/Co₂P/C-0.8 are composed of C-C/C=C, C-P/C-N and O-C=O. As shown in Figure 3F, the high-resolution N 1s spectrum exhibits three fitted peaks at 398.24 eV (pyridinic N), 399.22 eV (pyrrolic N), and 400.87 eV (graphitic N). This contributes significantly to enhancing electrical conductivity^[28,29].

To further analyze the charge transfer direction and quantity in the CoP/Co₂P heterostructure, the work function difference between CoP and Co₂P is calculated by density functional theory (DFT). Computational details are provided in Supporting information. As shown in Figure 4A, the work function value of CoP is 4.67 eV, which is lower than that of Co₂P at 4.93 eV, indicating a significant difference between the materials. In the CoP/Co₂P heterostructure model, the work function is further calculated [Figure 4B], which is situated

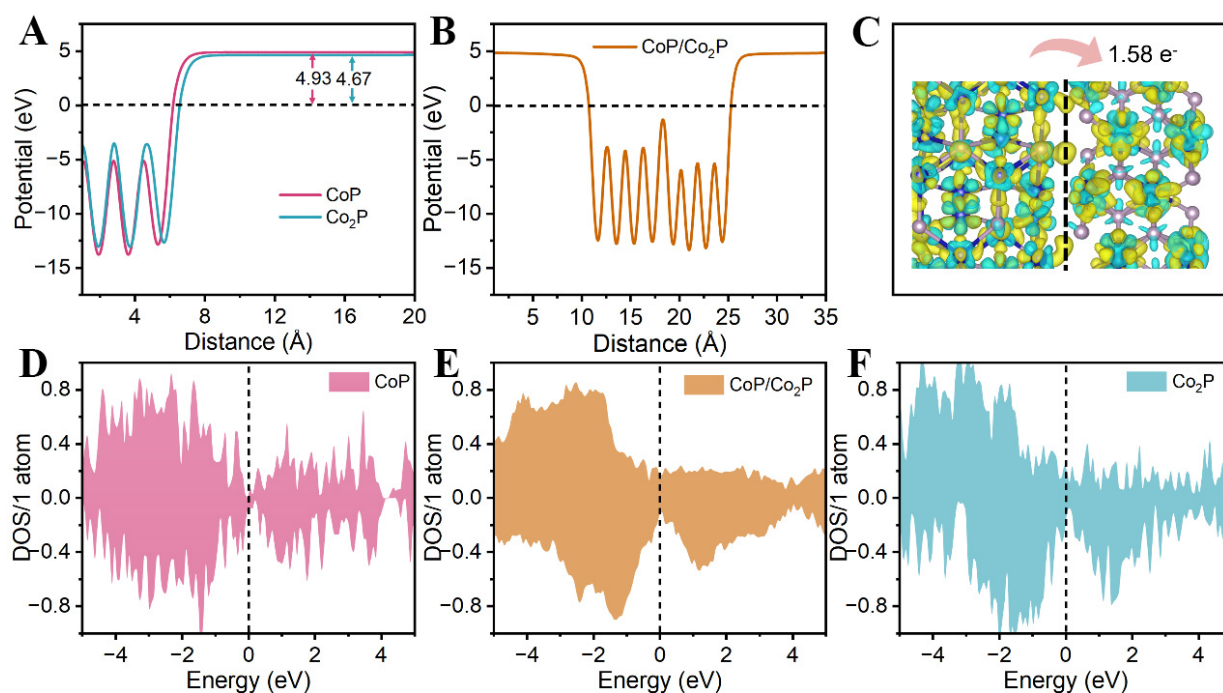


Figure 4. (A and B) The work functions of CoP, Co₂P and CoP/Co₂P heterostructure; (C) Bader charge and spin charge density differences of CoP/Co₂P heterostructure; (D–F) TDOS of CoP, CoP/Co₂P heterostructure and Co₂P. DOS: Density of states; TDOS: total density of states.

between CoP and Co₂P (4.82 eV). This is driven by the difference in the work function of the CoP and Co₂P. As demonstrated by the spin charge density differences and Bader charge analysis, it is clear that charge redistribution is evident at the interface of CoP/Co₂P [Figure 4C]. This results in a charge transfer of 1.58 eV electrons from Co₂P to CoP. The total density of states (TDOS) for CoP, CoP/Co₂P heterostructure and Co₂P are summarized in Figure 4D and E. The TDOS of CoP/Co₂P heterostructure also shows charge reconstruction upon building the heterostructure. Importantly, the occupancy around the Fermi level of the CoP/Co₂P heterostructure is comparable to that of Co₂P and significantly higher than CoP, indicating that the CoP/Co₂P heterostructure combines the great electronic conductivity of Co₂P with the high theoretical specific capacity of CoP.

The electrochemical performance of nanofibers as anode for LIBs is measured by assembling half-cells. Figure 5A shows the cyclic voltammetry (CV) curves of CoP/Co₂P/C-0.8 between 3.0 V and 0.01 V under 0.1 mV s⁻¹. In the first cathodic scan, the peak at 1.51 V corresponds to the electrochemical reaction of Li insertion into CoP/Co₂P to form Li_xCoP and Li_xCo₂P^[23,30]. Subsequently, the peak observed at 0.81 V, which disappears in subsequent cycles, corresponds to the formation of the solid electrolyte interphase (SEI) film^[31]. The peak observed at 0.66 V demonstrates the electrochemical reaction of lithiation of Li_xCoP and Li_xCo₂P into Li₃P and Co. During the subsequent charging process, peaks appear between 0.96 and 1.31 V, indicating that Co and Li₃P multiple conversion steps to reform CoP/Co₂P. During the second charge/discharge cycle, the reduction peaks shifted from 1.51 V and 0.66 V to 1.70 V and 0.73 V, respectively. This shift resulted from the irreversible phase transition, structural reorganization, and changes in interfacial impedance that occurred in CoP/Co₂P/C-0.8 during the first cycle. Most importantly, the CV curves in subsequent cycles of CoP/Co₂P/C-0.8 show good overlap, indicating excellent electrochemical reversibility and cycling stability. Furthermore, the CV curves of the other three nanofibers are similar to those of CoP/Co₂P/C-0.8 [Supplementary Figure 8A, 9A and 10A], suggesting they undergo comparable electrochemical processes during cycling.

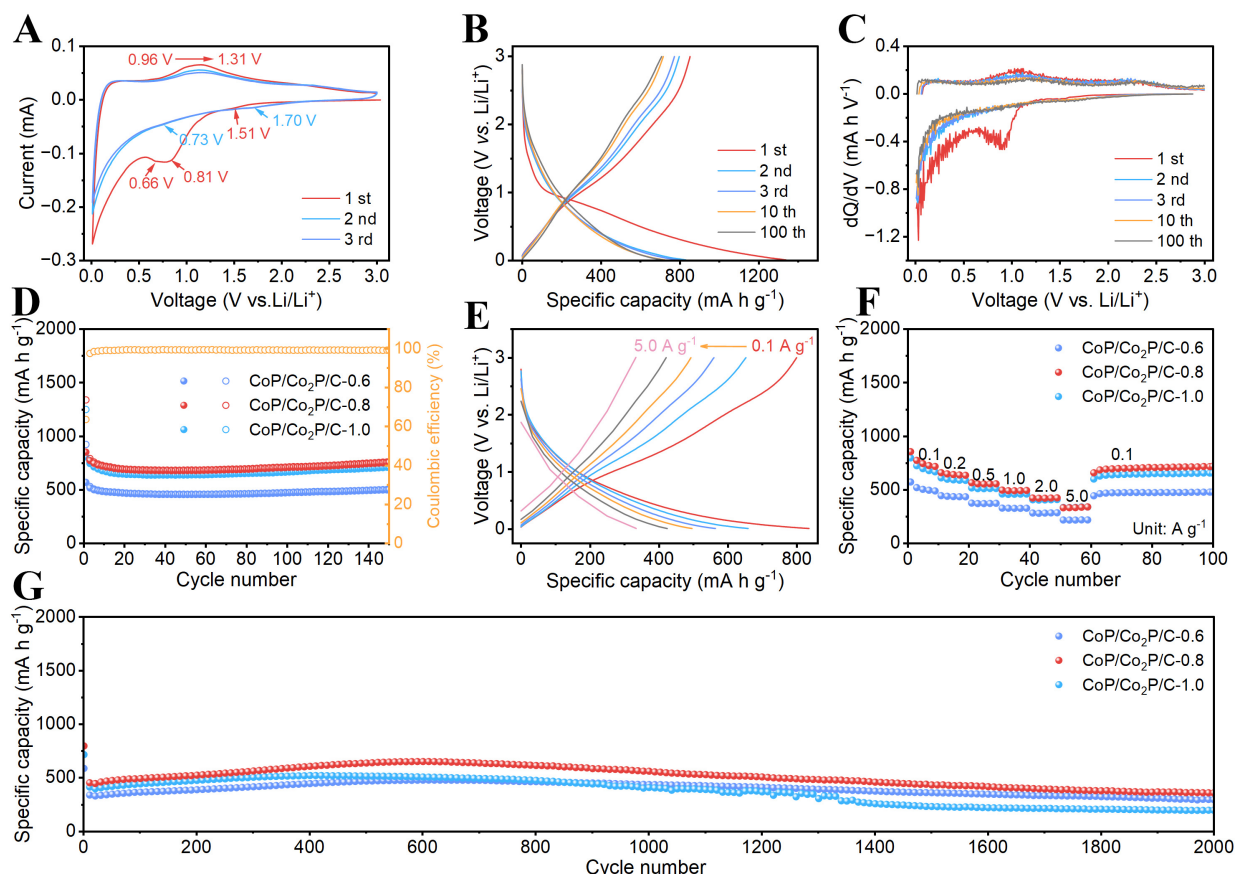


Figure 5. Electrochemical performance of CoP/Co₂P/C-0.8. (A) CV curves with the scan rate of 0.1 mV s⁻¹; (B) charge/discharge curves with the current density of 100 mA g⁻¹; (C) dQ/dV curves; (D) cycling performance of different nanofibers with the current density of 100 mA g⁻¹; (E) charge/discharge curves with different current densities; (F) rate capabilities and (G) cycling performances under 1,000 mA g⁻¹ of different nanofibers. CoP/Co₂P/C: CoP/Co₂P nanoparticles onto N, P co-doped carbon substrate; CV: cyclic voltammetry; dQ/dV: differential capacity.

The cycling performance of the nanofibers is evaluated at 100 mA g⁻¹. [Supplementary Figure 8B](#), [9B](#), [10B](#) and [Figure 5B](#) is the galvanostatic charge/discharge curves of nanofibers. The CoP/Co₂P/C-0.8 exhibited discharge and charge capacities of 1,339 and 852 mA h g⁻¹ in the first cycle, corresponding to Coulombic efficiency of 63.6%. This loss in the first cycle is mainly due to SEI formation and irreversible electrolyte decomposition and incomplete delithiation induced by electrode structure rearrangement^[32–33]. After the initial cycle, the charge/discharge curves remain stable, demonstrating excellent electrochemical reversibility, which is crucial for its cycling stability. [Figure 5C](#) shows the differential capacity (dQ/dV) curves of CoP/Co₂P/C-0.8. The positions of the redox peaks on this curve are similar to CV curves. Furthermore, after 100 cycles, the position of the redox peaks remained the same, showing that the electrochemical reaction of CoP/Co₂P/C-0.8 is reversible. Furthermore, the dQ/dV curves of CoP/C, CoP/Co₂P/C-0.6 and CoP/Co₂P/C-1.0 are similar to those of CoP/Co₂P/C-0.8 [[Supplementary Figure 8B](#), [9B](#) and [10B](#)]. [Figure 5D](#) and [Supplementary Figure 11A](#) shows the cycling performance of the four nanofibers at 100 mA g⁻¹. After 100 cycles, the specific capacity of the CoP/Co₂P/C-0.8 is 785 mA h g⁻¹, significantly exceeding that of the CoP/C (429 mA h g⁻¹), CoP/Co₂P/C-0.6 (503 mA h g⁻¹) and CoP/Co₂P/C-1.0 (716 mA h g⁻¹). The superior cycling performance of CoP/Co₂P/C-0.8 is mainly attributed to its optimal CoP and Co₂P ratios and CoP/Co₂P heterostructure. The high CoP ratio reduces the conductivity of nanofibers, preventing some active materials from joining electrochemical reactions and causing the decrease in specific capacity. However, the high Co₂P ratio reduces the theoretical specific capacity of nanofibers, resulting in lower specific capacity. Furthermore, the optimal CoP and Co₂P ratio introduces the appropriate number of

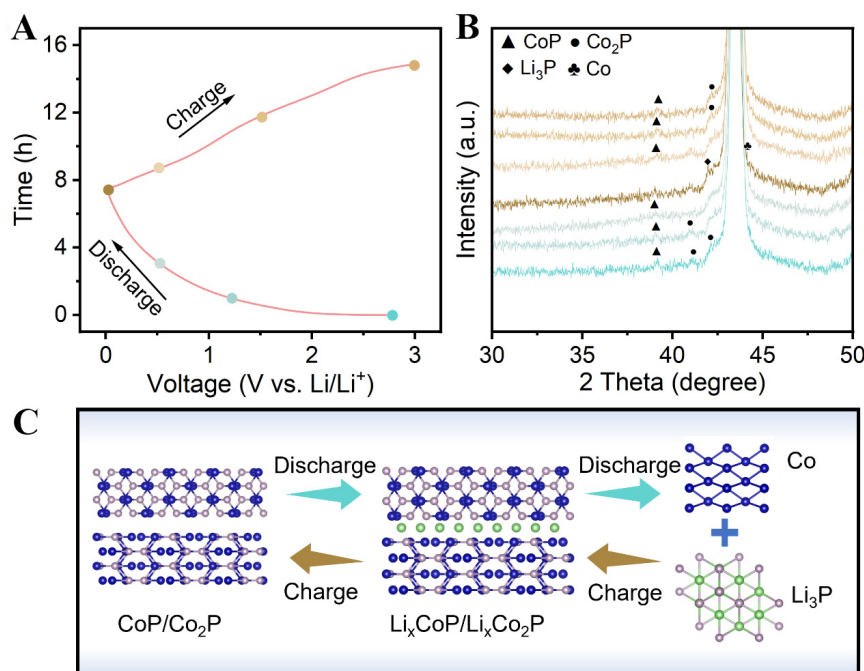


Figure 6. (A) Galvanostatic charge/discharge curves of CoP/Co₂P/C-0.8; (B) *Ex-situ* XRD patterns under different cycled states; (C) Schematic diagram of lithium storage mechanism of CoP/Co₂P/C nanofibers during the charge/discharge processes. CoP/Co₂P/C: CoP/Co₂P nanoparticles onto N, P co-doped carbon substrate; XRD: X-ray diffraction.

heterointerface, thereby creating more Li storage sites. To evaluate the rate performance of the four nanofibers, they are charged and discharged under various current densities. At different currents density, the plateau of the curve is not significantly shifted, and polarization is smaller, indicating that ion/electron transfer of CoP/Co₂P/C-0.8 is fast and the delithiation/lithiation process is stable and reversible [Figure 5E]. The rate performance of CoP/Co₂P/C nanofibers are shown in Figure 5F and Supplementary Figure 11B. The CoP/Co₂P/C-0.8 exhibits superior rate capability, with reversible capacities of 726, 643, 554, 491, 422, and 334 mA h g⁻¹ at increasing current densities from 100 to 5,000 mA g⁻¹, which is higher than that of CoP/C, CoP/Co₂P/C-0.6 and CoP/Co₂P/C-1.0. Importantly, the specific capacity recovers to 708 mA h g⁻¹ when the current density is restored to 100 mA h g⁻¹, demonstrating excellent rate performance. Then, the CoP/Co₂P/C is cycled under 1,000 mA g⁻¹ to evaluate its cycling life. After 2,000 cycles, CoP/Co₂P/C-0.8 retained the specific capacity exceeding 356 mAh g⁻¹, demonstrating outstanding cycling performance. Additionally, as shown in Supplementary Figure 12, CoP/Co₂P/C-0.8 maintains the nanofibers morphology after many cycles, suggesting that its heterostructure, smaller particle size, and abundant carbon effectively prevent electrode pulverization and agglomeration during cycles. This is a key reason for its outstanding electrochemical performance.

The lithiation mechanism of CoP/Co₂P/C-0.8 nanofibers is elucidated by *ex situ* XRD. Figure 6A and B shown the charge/discharge curves and *ex situ* XRD analysis results of the electrodes at different voltage states. The diffraction peaks before lithiation correspond to CoP and Co₂P. When discharge to 1.2 V, the diffraction peaks shift towards smaller angles, attributable to lattice expansion caused by Li⁺ insertion into the CoP and Co₂P lattices. When discharge continues to 0.5 V, the diffraction peaks shift further and the intensity weakens. Upon complete discharge to 0.01 V, the CoP and Co₂P phase disappear, forming Co and Li₃P phases. During subsequent charging cycles, the Li₃P and Co phases gradually disappear, while the CoP and Co₂P phases reform, indicating that the redox reaction is fully reversible. Based on the above analysis, the electrochemical mechanism of CoP is illustrated in Figure 6C. During the discharge stage, Li first inserts into the lattice of CoP and Co₂P, and finally forms Co and Li₃P. Importantly, the charging and discharging process is highly reversible.

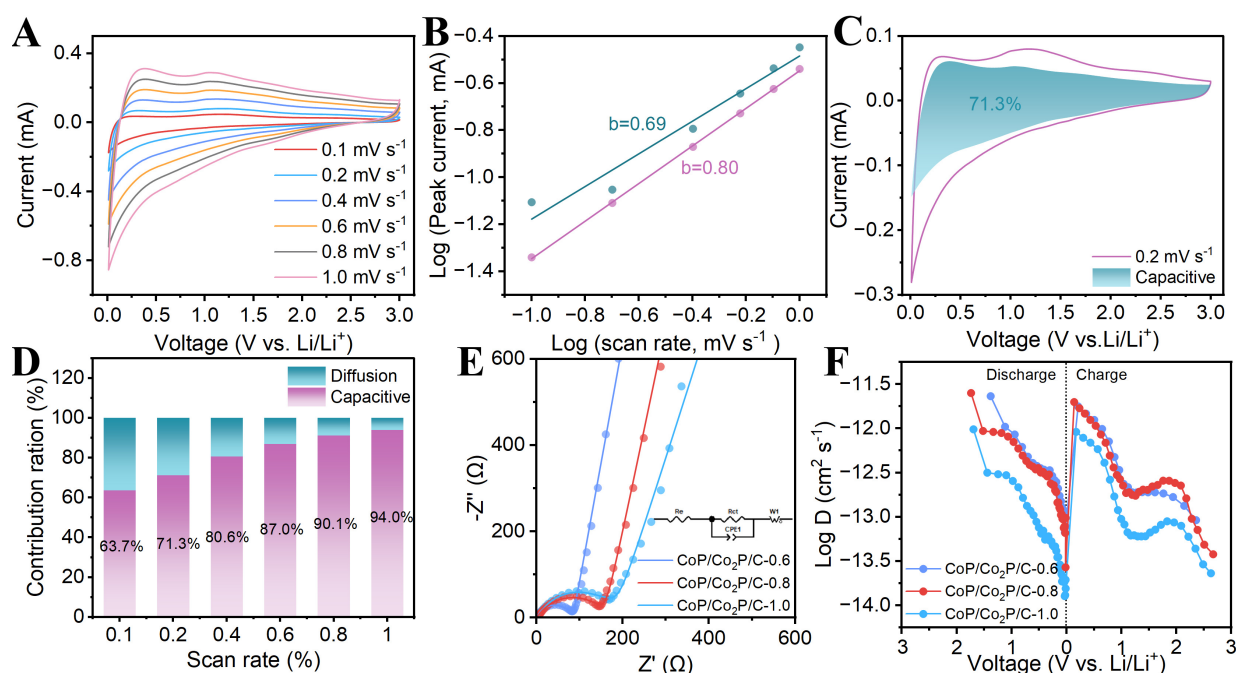


Figure 7. Electrochemical kinetic behavior analysis of CoP/Co₂P/C-0.8. (A) CV curve as the scan rate increases from 0.1 to 1.0 mV s⁻¹; (B) *b* values; (C) pseudo-capacitive contribution at 0.2 mV s⁻¹; (D) the values of pseudo-capacitive contribution at different scan rates; (E) EIS curves and (F) Li⁺ diffusion coefficients of different nanofibers. CoP/Co₂P/C: CoP/Co₂P nanoparticles onto N, P co-doped carbon substrate; EIS: electrochemical impedance spectroscopy.

To analyze the reasons for the differences in electrochemical performance of nanofibers, CV tests are performed on them at different scan rates. [Supplementary Figure 13A](#), [14A](#), [15A](#) and [Figure 7A](#) shows the CV curves of CoP/C and CoP/Co₂P/C nanofibers. For the CoP/Co₂P/C-0.8, the redox peaks are not disappeared with increasing of scan rate, only slightly shifted. This indicates that CoP/Co₂P/C-0.8 exhibits excellent ionic/electronic conductivity and fast Li⁺ storage kinetics. Additionally, the lithium storage mechanism of nanofibers is analyzed using the formula: $i = av^b$. Here, v denotes the scan rate, i denotes the peak current, a and b are constants. If $b = 0.5$, it indicates diffusion-controlled electrochemical reactions; $b = 1$ indicates capacitive-controlled lithium storage^[31,34]. For CoP/C and CoP/Co₂P/C nanofibers [[Supplementary Figure 13B](#), [14B](#), [15B](#) and [Figure 7B](#)], their b values all fall between 0.5 and 1, suggesting that Li⁺ storage processes is co-controlled by diffusion and capacitive. To calculate the ration of pseudo-capacitive contribution to the capacity, the formula: $i = k_1v + k_2v^{1/2}$ is employed for analysis. Here, k_1v represents the current contributed by pseudo-capacitance, while $k_2v^{1/2}$ denotes the current contributed by diffusion-controlled. At 0.2 mV s⁻¹, pseudo-capacitance contributes 71.3% of the capacity of CoP/Co₂P/C-0.8 [[Figure 7C](#)], which is exceeding than that of CoP/C, CoP/Co₂P/C-0.6 and CoP/Co₂P/C-1.0 [[Supplementary Figure 13C](#), [14C](#) and [15C](#)]. Moreover, for CoP/Co₂P/C-0.8 [[Figure 7D](#)] the pseudo-capacitive contribution progressively increased with rising scan rates, ultimately reaching 94%. This value is higher than CoP/C, CoP/Co₂P/C-0.6 and CoP/Co₂P/C-1.0. [[Supplementary Figure 13D](#), [14D](#) and [15D](#)]. This indicates that charge separation induced by BIEF can enhance the pseudo-capacitive contribution, thereby increasing lithium-ion diffusion rates and Li⁺ storage sites. [Figure 7E](#) is the electrochemical impedance spectroscopy (EIS) spectrum of three kinds of CoP/Co₂P nanofibers before cycling. After fitting, the charge transfer resistance (R_{ct}) of the three CoP/Co₂P/C nanofibers are 71.63, 139.3, and 152.2 Ω, respectively. As carbon content increases, the value of R_{ct} gradually rises, indicating that the conductive network formed by NPC optimizes the conductivity of nanofibers. Additionally, the impedance spectrum slopes of CoP/Co₂P/C-0.6 and CoP/Co₂P/C-0.8 in the low-frequency region are steeper than that of CoP/Co₂P/C-1.0, indicating superior Li⁺ diffusion performance. This is primarily attributed to the moderate ratio of CoP to Co₂P in the nanofibers,

which results in the formation of abundant heterointerface. These heterointerfaces provide rapid diffusion channels for Li^+ . The Li^+ diffusion coefficient (D_{Li^+}) is determined using the galvanostatic intermittent titration technique (GITT), with complete measurement conditions and the calculation process detailed in the [Supplementary Materials](#) [[Supplementary Figure 16](#)]. As demonstrated in [Figure 7F](#), among the three nanofibers, CoP/Co₂P/C-0.6 and CoP/Co₂P/C-0.8 exhibit higher D_{Li^+} . This is attributed to their optimized CoP/Co₂P ratio, which promotes the formation of more heterointerface. The BIEF generated by these heterointerface provides the rapid diffusion channels for Li^+ , which is the key reason for the outstanding rate performance exhibited by CoP/Co₂P/C-0.8.

CONCLUSIONS

In summary, nanofibers containing the CoP/Co₂P heterostructure and NPC are effectively prepared using electrospinning and reduction approaches. By controlling the ratio of Co^{2+} to PA in the electrospinning solution, the ratio of CoP and Co₂P as well as the number of heterointerface can be regulated. Owing to its novel heterogeneous structure, the CoP/Co₂P/C displays long cycle lifespan and rapid charge/discharge capability for use as the anode in LIBs. First, the NPC optimizes electronic conductivity and avoid pulverization caused by volume effects and enhance cycle stability. Second, the optimal ratio of CoP and Co₂P successfully balances high capacity with high conductivity. Finally, the strong coupling between CoP and Co₂P within the nanofibers generates abundant defects and BIEF, which creates active sites and Li^+ diffusion channels, thereby enhancing electrochemical performance of nanofibers. This work demonstrates that introducing an appropriate number of CoP/Co₂P heterostructure can effectively enhance their electrochemical performance, which is expected to be applicable in the design of other high-performance anodes.

DECLARATIONS

Authors' contributions

Conceived the idea, conducted part of the experiments, and wrote the manuscript: Wang, X.

Carried out electrochemical performance measurements: Yue, C.

Synthesized the sample: Wang, W.

Verified the data and revised the manuscript: Yao, F.; Zhu, W.

Characterized the samples: Li, J.

Supervised the project: Nie, P.; Chang, L.

All authors discussed the results and contributed to the revision and finalization of the manuscript.

Availability of data and materials

Some results of supporting the study are presented in the [Supplementary Materials](#).

AI and AI-assisted tools statement

Not applicable.

Financial support and sponsorship

This work was supported by the Natural Science Foundation of Jilin Province (YDZJ202301ZYTS296), National Natural Science Foundation of China (52501281), the Research Program on Science and Technology from the Education Department of Jilin Province (JJKH20240558KJ).

Conflicts of interest

All authors declared that there are no conflicts of interest.

Ethical approval and consent to participate

Not applicable.

Consent for publication

Not applicable.

Copyright

© The Author(s) 2026.

Supplementary Materials

[Supplementary Materials](#)

REFERENCES

- Huang, X. Y.; Zhao, C. Z.; Kong, W. J.; et al. Tailoring polymer electrolyte solvation for 600 Wh kg⁻¹ lithium batteries. *Nature* **2025**, *646*, 343-50. DOI PubMed
- Wu, D.; Liu, Q.; Zhu, Q.; et al. Fast-charging li-ion battery enabled by an acetonitrile-based electrolyte. *ACS. Energy. Lett.* **2025**, *10*, 4911-8. DOI
- Xiao, Z.; Wu, H.; Quan, L.; et al. Micro-sized CVD-derived Si-C anodes: challenges, strategies, and prospects for next-generation high-energy lithium-ion batteries. *Energy. Environ. Sci.* **2025**, *18*, 4037-52. DOI
- Sharma, G. K.; Elkins, J.; Puthirath, A. B.; et al. Binder-free MoO₂-MoO₃ nanoarrays as high-performance anodes for Li-Ion batteries. *Small* **2025**, *21*, e2500361. DOI PubMed
- Li, Z.; Zhang, Z.; Liao, H.; Zheng, Y.; Gao, Y. Anode materials for proton batteries: progress and prospects. *ACS. Nano.* **2025**, *19*, 12680-709. DOI PubMed
- Liu, Y.; Hu, Q.; Shi, Q.; et al. Green synthesis of Cu₃P to achieve low-temperature and high initial coulombic efficiency sodium ion storage. *Adv. Energy. Mater.* **2025**, *15*, 2500723. DOI
- Lan, X.; Li, Z.; Zeng, Y.; Han, C.; Peng, J.; Cheng, H. M. Phosphorus-based anodes for fast-charging alkali metal ion batteries. *EcoMat* **2024**, *6*, e12452. DOI
- Li, W.; Li, Y.; Wang, J.; et al. Generic synthesis of high-entropy phosphides for fast and stable Li-ion storage. *Energy. Environ. Sci.* **2024**, *17*, 5387-98. DOI
- Li, W.; Wang, J. H.; Yang, L.; et al. High-entropy engineering of cubic SiP with metallic conductivity for fast and durable Li-ion batteries. *Adv. Mater.* **2024**, *36*, e2314054. DOI PubMed
- Zhu, H.; Li, W.; Yang, K.; Zhang, L.; Sun, L. One-step thermal synthesis of FeP nanoparticles highly-dispersed into a porous NPPCG framework for enhanced lithium storage. *J.. Energy. Storage.* **2025**, *112*, 115595. DOI
- Zhou, Y.; Wang, Y.; Zhang, Y.; et al. Abundant Cu₃P/Co₂P/CoP@NC heterostructures boost charge transfer toward fast and durable sodium storage. *Carbon. Energy.* **2025**, *7*, e721. DOI
- Zeng, H.; Liu, R.; Wu, Q.; et al. Naturalized bioreactor assisted fabrication of ferrous(II) phosphate nanodots decorated in carbon for “fast-charging” lithium-ion batteries. *Adv. Funct. Mater.* **2025**, *35*, 2503614. DOI
- Liu, J.; Li, B.; Mu, P.; et al. Fabricating 3D network for FeP@MXene toward stable and high-capacity lithium-ion storage. *Small. Methods.* **2025**, *9*, e2500185. DOI PubMed
- Fan, Z.; Wang, J.; Wu, Y.; Zhang, P. Advanced high-entropy materials for high-quality energy storage and conversion. *Energy. Storage. Mater.* **2025**, *74*, 103954. DOI
- Shi, H.; Zhang, Y.; Li, X.; et al. Ordered design of N-doped carbon fiber hybrid bilayer skeleton for controlled bottom-up Na plating/stripping toward anode-less sodium metal batteries. *Chem. Eng. J.* **2025**, *519*, 165444. DOI
- Yuan, F.; Li, Z.; Wang, Q.; et al. sp² configuration coupled vacancy rich carbon enables excellent low potential potassium storage. *Energy. Storage. Mater.* **2025**, *76*, 104119. DOI
- Islam, T.; Bayat, S.; Wright, M. A.; et al. Porous and amorphous Mn₄Mo₃S₁₃ chalcogel electrode for high-capacity conversion-based lithium-ion batteries. *J. Am. Chem. Soc.* **2025**, *147*, 7400-10. DOI PubMed
- Zhang, M.; Xiao, H.; Liu, Y.; et al. Interfacial build-in electric field unlocking hetero-architected CoO-Co₃O₄ nanotubes toward high-performance Li-S batteries. *Adv. Funct. Mater.* **2025**, *36*, e20708. DOI
- Xiao, S.; Chen, Y.; Zhou, X.; et al. Hierarchical phosphide-based hybrid anodes for high-performance lithium-ion batteries. *Nano. Lett.* **2025**, *25*, 3532-40. DOI PubMed
- Li, J.; Li, C.; Hu, Y.; et al. Long-lasting lithium-ion batteries enabled by advanced anode design of a hydrangea-like FeP/SnP@C heterostructure. *ACS. Appl. Mater. Interfaces.* **2025**, *17*, 12085-94. DOI PubMed
- Hao, Z.; Liu, D.; Zuo, X.; Yu, H.; You, T.; Zhang, Y. Built-In Electric Field Induced Uniform Li Deposition via Construction of CoP/Co₃P Heterojunction in 3D Carbon Nanofiber Networks. *Adv. Funct. Mater.* **2024**, *35*, 2415251. DOI

22. An, Y.; Pei, Z.; Luan, D.; Lou, X. W. D. Foldable anode-free sodium batteries enabled by N,P-codoped carbon macroporous fibers incorporated with CoP nanoparticles. *Sci. Adv.* **2025**, *11*, eadv2007. DOI PubMed PMC
23. Li, S.; Xu, Y.; Zhang, X.; et al. CoP Quantum dots embedded in carbon polyhedra through Co-P-C bonding enabling high-energy lithium-ion capacitors. *Adv. Funct. Mater.* **2024**, *34*, 2314870. DOI
24. Zhang, H.; Pang, M.; Yang, M.; et al. Constructing three-dimensional porous SnS₂/rGO as superior-rate and long-life anodes for lithium-ion batteries. *Langmuir* **2025**, *41*, 876-84. DOI PubMed
25. Wang, X.; Xu, Y. J.; Wu, X. S.; Ma, M. W.; Tian, Y.; Su, Z. M. Nitrogen-doped Co₃O₄@porous carbon derived from metal-organic frameworks for high-performance lithium ion batteries. *Langmuir* **2025**, *41*, 10782-8. DOI PubMed
26. Liu, L.; Xie, H.; Zheng, Y.; et al. Multicomponent Anodes Based on Amorphous ZnP₂ for Fast-Charging/Discharging Lithium-Ion Batteries. *Advanced. Energy. Materials.* **2024**, *15*, 2404900. DOI
27. Lu, Y.; Kang, Q.; Dong, F.; et al. Metalloid phosphorus induces tunable defect engineering in high entropy oxide toward advanced lithium-ion batteries. *Adv. Funct. Mater.* **2024**, *35*, 2413782. DOI
28. Li, X.; Guan, G.; Tong, S.; et al. Two birds with one stone: Bimetallic ZnCo₂S₄ polyhedral nanoparticles decorated porous N-doped carbon nanofiber membranes for free-standing flexible anodes and microwave absorption. *J. Colloid. Interface. Sci.* **2025**, *678*, 1031-42. DOI PubMed
29. Chen, B.; Cao, T.; Yu, Y.; et al. Rational design of yolk-shell Fe₇S₈@C-N for high rate and long cycle Li-Ion batteries. *Nano. Lett.* **2025**, *25*, 10279-86. DOI PubMed
30. Tan, W.; Liu, Z.; Wu, Q.; et al. Flexible free-standing Fe-CoP-NAs/CC nanoarrays for high-performance full lithium-ion batteries. *J. Colloid. Interface. Sci.* **2024**, *667*, 441-9. DOI PubMed
31. Yu, J.; He, Y.; Li, J.; et al. *In-situ* rooting biconical-nanorods-like Co-doped FeP @carbon architectures toward enhanced lithium storage performance. *Chem. Eng. J.* **2023**, *477*, 146996. DOI
32. Liu, X.; Yu, Y.; Li, K.; et al. Intergrating hollow multishelled structure and high entropy engineering toward enhanced mechano-electrochemical properties in lithium battery. *Adv. Mater.* **2024**, *36*, e2312583. DOI PubMed
33. Ou, H.; Huang, M.; Li, P.; et al. Tailoring and understanding the lithium storage performance of triple-doped cobalt phosphide composites. *J. Colloid. Interface. Sci.* **2024**, *672*, 753-64. DOI PubMed
34. Huang, L.; Huang, Y.; Wang, J.; et al. Synergistic dual-carbon networks bridged Mn-doped TiNb₂O₇ anode for fast-charging lithium-ion batteries. *ACS. Appl. Mater. Interfaces.* **2025**, *17*, 53659-69. DOI PubMed

Disclaimer/Publisher's Note: All statements, opinions, and data contained in this publication are solely those of the individual author(s) and contributor(s) and do not necessarily reflect those of OAE and/or the editor(s). OAE and/or the editor(s) disclaim any responsibility for harm to persons or property resulting from the use of any ideas, methods, instructions, or products mentioned in the content.



© The Author(s) 2026. Open Access This article is licensed under a Creative Commons Attribution 4.0 International License (<https://creativecommons.org/licenses/by/4.0/>), which permits unrestricted use, sharing, adaptation, distribution and reproduction in any medium or format, for any purpose, even commercially, as long as you give appropriate credit to the original author(s) and the source, provide a link to the Creative Commons license, and indicate if changes were made.